Pacific contribution to the early 20th century warming in the Arctic

Lea Svendsen[1]*, Noel Keenlyside[1,2], Ingo Bethke[3], Yongqi Gao[2,4] and Nour-Eddine Omrani[1]

[1]Geophysical Institute, University of Bergen, and Bjerknes Centre for Climate Research, Bergen, Norway

[2]Nansen Environmental and Remote Sensing Center and Bjerknes Centre for Climate Research, Bergen, Norway

[3]Uni Research Climate and Bjerknes Centre for Climate Research, Bergen, Norway

[4]Nansen-Zhu International Research Center, Institute of Atmospheric Physics, Chinese Academy of Science, Beijing, China

*e-mail: lea.svendsen@uib.no

Arctic surface temperature warmed more than twice as fast as global temperature during the early 20th century, similar to during the recent global warming. This Arctic warming has been attributed to both external forcing[1] and internal variability associated with atmospheric dynamics[2,3] and Atlantic Ocean temperature[4] in combination with Pacific variability[5]. Here we show that Pacific decadal variability alone was a key contributor to the early 20th century Arctic warming, through coupled climate model experiments that superpose externally forced and dynamically driven changes. Sea surface temperatures (SST) in the model are phased to observations by prescribing historical wind variations over the Pacific, driving thermodynamically consistent decadal variations. During the early 20th century, the Pacific Decadal Oscillation (PDO) transitioned to a positive phase with concomitant deepening of the Aleutian Low warming the Arctic by poleward low-level advection of extra-tropical air. In addition, our experiments reveal that the implemented Pacific surface changes weaken the polar vortex leading to subsidence-induced adiabatic heating of the Arctic surface. Thus, our results suggest that the observed recent shift to the positive PDO phase[6] will intensify Arctic warming in the forthcoming decades.

Observational records show two periods of enhanced decadal warming in the Arctic during the instrumental period: the early 20th century warming between 1910 and the early 1940s, and the later warming period starting in the 1970s (Supplementary Fig. 1). These warming periods coincided with enhanced warming globally. The earlier increase in global temperature has been explained by a combination of anthropogenic and natural external forcing factors[7]. However, coupled climate models underestimate this warming possibly due to phasing of internal variability[8]. Both the phasing of Atlantic multi-decadal variability (AMV) and the PDO have been suggested as important reasons for accelerating and decelerating global surface temperature trends[8-13]. Earlier studies on the topic have focused on the impact of the Atlantic[8,9], but the PDO has earned attention related to the recent so-called ‘hiatus’ in the global surface temperature trend[14]. In addition, Pacific SSTs have been shown to impact interannual variability[15] and recent trends in the Arctic[16] as well as modulate Arctic Amplification[6]. Another recent paper suggested a combination of the positive phase of both AMV and PDO could have intensified the early 20th century warming of the high latitude Northern Hemisphere land surface[5], but did not isolate the PDO contribution. Moreover, the use of prescribed SST and sea ice conditions in earlier studies precluded detailed consideration of the energetics that lead to the Arctic warming and the amplifying role of sea ice feedbacks. We hypothesize that the negative-to-positive shift of the PDO (Supplementary Fig. 2) could have played a key role in the early 20th century Arctic warming, and we propose a new mechanism for how this could come about.

To investigate how decadal variability in the Pacific could have contributed to the early 20th century Arctic warming, we have performed two six-member ensemble experiments with the Norwegian Earth System Model (NorESM)[17] including transient 20th century forcing. The first ensemble, a control experiment (CNTRL), is a fully coupled historical simulation as done for the Coupled Model Inter-Comparison Project 5 (CMIP5). The second ensemble (TAU-PAC) is partially coupled by prescribing momentum flux anomalies[18] from reanalysis[19] to the Indo-Pacific Ocean. By using this method, we constrain the phasing of variability over the Pacific Ocean and reproduce the observed phase changes of the PDO (Supplementary Fig. 2), while the AMV remains largely unaffected in our model. At the same time the model maintains an active thermodynamic coupling. It is therefore an energetically consistent alternative for investigating the dynamics of the early 20th century warming to standard SST-restoring 'pacemaker' experiments[10]. Both ensembles include the same transient external forcing, and although some non-linear interactions may exist between external forcing and the response of the climate system to the imposed winds as with standard SST 'pacemaker' experiments[10], we can use this experimental setup to separate the impact of dynamical driven ocean changes in the Pacific from the direct radiative forced changes (see Methods).

During the early 20th century the Arctic (ocean and land surface north of 70°N) warms by around 1.1 K from the minimum between the years 1911-1920 to the peak between 1936-1945 (Fig. 1). At the same time Northern Hemisphere surface temperatures increase by around 0.5 K. TAU-PAC captures well this Northern Hemisphere warming trend and year to year variations (Supplementary Fig. 3). TAU-PAC also manages to capture the observed early 20th century Arctic warming trend of 1.1K (ensemble range: 0.82-1.71K) and is significantly warmer than CNTRL in the later part of this period. Radiative forcing leads to a warming of only 0.45K in CNTRL, underestimating the early 20th century Arctic warming by more than 50% (ensemble range: 0.04-0.80K), consistent with earlier studies[2,8]. The early 20th century Arctic warming is strongest during the cold season, and we therefore focus on the months from October to February (ONDJF) (Fig. 1c). The seasonality is somewhat weaker in the experiments compared to observations, possibly related to a weaker seasonal cycle of sea ice extent in NorESM[17]. It is however clear that by constraining SST variability in the Pacific we reproduce the observed early 20th century Arctic warming.

The enhanced early 20th century Arctic warming in TAU-PAC is also seen in the trend patterns of winter surface temperature (Fig. 2a-c). The warming pattern in TAU-PAC is similar to observed and significantly stronger than the warming in CNTRL (Supplementary Fig. 4). These results are largely independent of the choice of endpoints and averaging periods between 1910 and 1945. However, observational data are scarce over the majority of the Arctic Ocean during this period, especially during winter. This, together with internal atmospheric variability, may account for discrepancies between observed and simulated trend patterns. The Arctic warming is accompanied by a weak warming in the tropical North Atlantic, and a stronger warming in the northern North Pacific and the tropical Pacific (Fig. 2). The tropical Pacific warms between 15-25°N, but because of poor data coverage in the equatorial region during this period, observed data products seem to underestimate the equatorial Pacific warming in the early 1940s[5,13]. On the other hand, TAU-PAC simulates equatorial Pacific warming but no warming in the subtropics. This could be because the meridional width of the Pacific cold tongue is too narrow in NorESM[17]. Nevertheless, the SST changes in both observations and TAU-PAC project upon a cold-to-warm PDO shift (Supplementary Fig. 2b). These results suggest that by dynamically constraining the Pacific Ocean we can account for the observed Arctic warming that cannot be directly explained by external forcing simulated in CNTRL.

During the early 20th century warming period in TAU-PAC, the northward energy transport increases, primarily due to increased atmospheric transport (Supplementary Fig. 5). As the Arctic warms, sea level pressure (SLP) decreases near the Aleutian Islands in the North Pacific (Fig. 2f), indicative of a deepening Aleutian Low. During the early 20th century warming period the North Pacific-index[20] describing the variability of the Aleutian Low shifts from positive to negative (Supplementary Fig. 6). This tendency is reproduced in TAU-PAC. However large uncertainties exist in observed SLP data in the North Pacific during this period[21]. Aleutian Low variations can act as a boundary condition constraining internal variability in the Arctic atmospheric circulation[22]. In addition, the deepening Aleutian Low is consistent with increased horizontal heat advection into the Arctic[5].

A decomposition of the temperature tendency at lower levels (1000-700hPa) over the Arctic (see Methods) shows that not only low-level horizontal advection, but also subsidence-induced adiabatic heating, contributes to the early 20th century Arctic warming in TAU-PAC (Supplementary Fig. 7). The subsidence occurs in association with a weakening polar stratospheric vortex (Fig. 3) and the associated stratosphere/troposphere coupling[23]. Although the downward stratosphere-troposphere coupling is well accepted, the associated mechanisms remain disputed[24]. Several mechanisms have been proposed including: the non-local downward control of the tropospheric circulation by stratospheric wave forcing, diabatic forcing and potential vorticity change, wave reflection and refraction, as well as eddy feedbacks in the troposphere[24]. We find that the deepening Aleutian Low during the warming period, and associated strengthening of the Asian trough and the ridge over the eastern North Pacific (Fig. 4b, d), strengthens the amplitude of wave number one by about 20% (Fig 4f), and there is positive interference between the perturbed and background stationary wave with a spatial correlation of 0.96 in TAU-PAC (the correlation in CNTRL is -0.76). The westward wave-tilt with height suggests upwards propagating waves that weaken the high latitude westerlies and the polar vortex (Fig. 4f). This mechanism is similar to the atmospheric response to El Niño events[25]. The positive SLP trend over the Arctic consistent with adiabatic heating is, however, not present in the observed data (Fig. 2d), although hardly any SLP measurements exist in the Arctic before the 1950s[26].

While the advection term can cause the warming on the Pacific side of the Arctic, the adiabatic heating is not necessarily bound to the Pacific side. The associated surface wind changes (Supplementary Fig. 8) can for instance explain the maximum warming in the Barents Sea region by increasing the transport of warm Atlantic water into this region and reducing the sea ice extent here[3].

The overall early 20th century Arctic temperature trend results from several shorter periods of warming (Fig 1b and Supplementary Fig. 7). The heating by advection occurs when the Aleutian Low deepens (Supplementary Fig. 6). The adiabatic heating events, on the other hand, coincide with the minima of the Aleutian Low (Supplementary Fig. 6) and periods of pronounced warming in the tropical Pacific (Supplementary Fig. 9). To investigate if the deepening of the Aleutian Low and the Arctic warming are forced by the warming events in the tropical Pacific alone, or if the changes in the extratropical Pacific sea surface contribute as well, we have performed two additional ensemble experiments: TROP and XTROP. In these ensembles we prescribe momentum flux only over the tropical Pacific and the extratropical Pacific, respectively. The full extent of the Arctic warming seen in TAU-PAC is not reproduced in either of the additional ensembles (Fig. 5a, e). However, both ensembles simulate a deepening Aleutian Low (Fig. 5b, f), albeit weaker than in TAU-PAC. This signal protrudes through the mid-troposphere (Fig. 5c, g), while the pattern at upper levels is weaker (Fig. 5d, h). Therefore, we conclude that the low-level heat advection and subsidence-induced adiabatic heating that warms the Arctic in TAU-PAC is a result of a combination of tropical and extratropical Pacific forcing, including tropical-extratropical interactions.

Our CNTRL ensemble indicates that radiative forcing can explain half of the warming in the early 20th century by warming the Arctic surface directly or indirectly through for instance warming of the Atlantic Ocean. We find that the other half of the observed Arctic temperature increase is dynamically forced through decadal variability in the tropical and extratropical Pacific. A non-radiative Atlantic forcing effect has not been included in this study, and therefore, we cannot exclude the possibility that a part of the early 20th century warming could potentially also be attributed to a phase change of the AMV. Albeit the Pacific forces some warming in the North Atlantic in TAU-PAC (Fig. 2c and 5a, e) through interbasin teleconnections between the Pacific and the tropical North Atlantic (Supplementary Fig. 2d) that could potentially contribute to the Arctic warming during this period. However, we link the main drivers for the non-radiative Arctic warming in this period directly to the implemented changes in the Pacific.

Since we can reproduce the early 20th century warming without a pronounced AMV signal, we propose that the phasing of decadal variability in the Pacific played a major role in the early 20th century Arctic warming. However, the wind stress anomalies we prescribe over the Pacific could potentially be forced by the Atlantic[27]. In addition external forcing has been shown to phase decadal variability over the oceans in some models[28]. Such results are model dependent; NorESM could be less sensitive to external forcing or could have a stronger link between the Pacific and the Arctic than other models. As observations are limited for the early 20th century warming period, it is difficult to assess the veracity of our simulations. Therefore, it is important to perform similar experiments with other models and forced by different reanalysis products to understand the model and data dependency of these results. Nevertheless, the results presented here propose a plausible mechanism involving both radiative forcing and decadal variability in the Pacific for the cause of a warming in the Arctic of the size indicated by available observations.

The results from this study imply that the warmer Pacific SSTs associated with a positive PDO in the 1980s could have enhanced the warming in the Arctic attributed to an Arctic amplification of anthropogenic-forced global warming. We speculate that the present positive PDO conditions[6] may cause the Arctic to warm at an even higher rate in the forthcoming decades, although internal atmospheric variability and the phasing of AMV, as well as the secondary effects of the PDO Arctic Amplification[6] might offset it. Such PDO impacts on the Arctic are important and need to be taken into account when evaluating future climate predictions and projections.

References

1 Suo, L., Otterå, O. H., Bentsen, M., Gao, Y. & Johannessen, O. M. External forcing of the early 20th century Arctic warming. *Tellus A* **65**, (2013).

2 Wang, M. *et al.* Intrinsic versus Forced Variation in Coupled Climate Model Simulations over the Arctic during the Twentieth Century. *Journal of Climate* **20**, 1093-1107, (2007).

3 Bengtsson, L., Semenov, V. A. & Johannessen, O. M. The Early Twentieth-Century Warming in the Arctic—A Possible Mechanism. *Journal of Climate* **17**, 4045-4057,(2004).

4 Johannessen, O. M., Kuzmina, S. I., Bobylev, L. P. & Miles, M. W. Surface air temperature variability and trends in the Arctic: new amplification assessment and regionalisation. *Tellus A* **68**, (2016).

5 Tokinaga, H., Xie, S.-P. & Mukougawa, H. Early 20th-century Arctic warming intensified by Pacific and Atlantic multidecadal variability. *Proceedings of the National Academy of Sciences* **114**, (2017).

6 Screen, J. A. & Francis, J. A. Contribution of sea-ice loss to Arctic amplification is regulated by Pacific Ocean decadal variability. *Nature Clim. Change* **6**, 856-860 (2016).

7 Tett, S. F. B., Stott, P. A., Allen, M. R., Ingram, W. J. & Mitchell, J. F. B. Causes of twentieth-century temperature change near the Earth's surface. *Nature* **399**, 569-572 (1999).

8 Delworth, T. L. & Knutson, T. R. Simulation of Early 20th Century Global Warming. *Science* **287**, 2246-2250 (2000).

9 Schlesinger, M. E. & Ramankutty, N. An oscillation in the global climate system of period 65-70 years. *Nature* **367**, 723-726 (1994).

10 Kosaka, Y. & Xie, S.-P. The tropical Pacific as a key pacemaker of the variable rates of global warming. *Nature Geosci* **9**, 669-673 (2016).

11 Steinman, B. A., Mann, M. E. & Miller, S. K. Atlantic and Pacific multidecadal oscillations and Northern Hemisphere temperatures. *Science* **347**, 988-991 (2015).

12 Dai, A., Fyfe, J. C., Xie, S.-P. & Dai, X. Decadal modulation of global surface temperature by internal climate variability. *Nature Clim. Change* **5**, 555-559 (2015).

13 Thompson, D. M., Cole, J. E., Shen, G. T., Tudhope, A. W. & Meehl, G. A. Early twentieth-century warming linked to tropical Pacific wind strength. *Nature Geosci* **8**, 117-121, (2015).

14 Kosaka, Y. & Xie, S.-P. Recent global-warming hiatus tied to equatorial Pacific surface cooling. *Nature* **501**, 403-407 (2013).

15 Hu, C. *et al.* Shifting El Niño inhibits summer Arctic warming and Arctic sea-ice melting over the Canada Basin. *Nature Communications* **7**, 11721 (2016).

16 Li, F., Wang, H. & Gao, Y. Extratropical Ocean Warming and Winter Arctic Sea Ice Cover since the 1990s. *Journal of Climate* **28**, 5510-5522 (2015).

17 Bentsen, M. *et al.* The Norwegian Earth System Model, NorESM1-M - Part 1: Description and basic evaluation of the physical climate. *Geoscientific Model Development* **6**, 687-720 (2013).

18 Ding, H. *et al.* The variability of the East Asian summer monsoon and its relationship to ENSO in a partially coupled climate model. *Climate Dynamics* **42**, 367-379 (2014).

19 Compo, G. P. *et al.* The Twentieth Century Reanalysis Project. *Quarterly Journal of the Royal Meteorological Society* **137**, 1-28 (2011).

20 Trenberth, K. E. & Hurrell, J. W. Decadal atmosphere-ocean variations in the Pacific. *Climate Dynamics* **9**, 303-319 (1994).

21 Hetzinger, S. *et al.* Marine proxy evidence linking decadal North Pacific and Atlantic climate. *Climate Dynamics* **39**, 1447-1455 (2012).

22 Sein, D. V., Koldunov, N. V., Pinto, J. G. & Cabos, W. Sensitivity of simulated regional Arctic climate to the choice of coupled model domain. *Tellus A* **66**, (2014).

23 Ambaum, M. H. P. & Hoskins, B. J. The NAO Troposphere–Stratosphere Connection. *Journal of Climate* **15**, 1969-1978 (2002).

24 Haynes, P. Stratospheric Dynamics. *Annual Review of Fluid Mechanics* **37**, 263-293 (2005).

25 Ineson, S. & Scaife, A. A. The role of the stratosphere in the European climate response to El Niño. *Nature Geoscience* **2**, 32 (2008).

26 Allan, R. & Ansell, T. A New Globally Complete Monthly Historical Gridded Mean Sea Level Pressure Dataset (HadSLP2): 1850–2004. *Journal of Climate* **19**, 5816-5842 (2006).

27 Zhang, R. & Delworth, T. L. Impact of the Atlantic Multidecadal Oscillation on North Pacific climate variability. *Geophysical Research Letters* **34**, (2007).

28 Otterå, O. H., Bentsen, M., Drange, H. & Suo, L. External forcing as a metronome for Atlantic multidecadal variability. *Nature Geosci* **3**, 688-694 (2010).

29 Smith, T. M. & Reynolds, R. W. Improved Extended Reconstruction of SST (1854–1997). *Journal of Climate* **17**, 2466-2477 (2004).

30 Hansen, J., Ruedy, R., Sato, M. & Lo, K. Global surface temperature change. *Reviews of Geophysics* **48**, (2010).

Methods

For our experiments, we have used the Norwegian Earth System Model (NorESM). NorESM consists of the atmospheric component CAM4-Oslo, the ocean component MICOM, the land component CLM4, the sea ice model CICE4, and the coupler CPL7. NorESM is based on the Community Earth System Model (CESM1)[31] with the same land and sea ice components and coupler but differs in the following aspects. NorESM uses an isopycnic coordinate ocean general circulation model developed from MICOM[32] and the atmosphere component includes a different chemistry-aerosol-cloud-radiation interaction scheme. The NorESM1-ME version used here also includes prognostic biochemical cycling, which is deactivated in this study. Here we use the CMIP5 version of the model[17,33].

We performed six-member ensembles with NorESM with transient 20th century historical forcing. After year 2006 forcing given by RCP4.5[34] is used. First, we have a control ensemble (CNTRL) with six members of fully coupled historical simulations as done for the CMIP5[35]. We initialize the historical simulations at year 1850 with initial conditions given by a preindustrial control simulation. The initial conditions are selected at a 10-year interval from the preindustrial control simulation.

The second ensemble simulation (TAU-PAC) is partially coupled, similar to the setup from Ding et al. (Ref.18). Here we prescribe daily momentum flux anomalies from the NOAA-CIRES 20th Century Reanalysis data version 2 (20CR)[19] provided by the NOAA/OAR/ESRL PSD, Boulder, Colorado, USA, from their web site at http://www.esrl.noaa.gov/psd/ to the ocean component of the model between 25°S and 60°N in the Indo-Pacific. Otherwise the model is fully coupled. We have a tapering region of linear weighting of 5° latitude outside the latitudinal boundaries, at the Bering Strait in the north and at the southern tip of Africa in the south. In grid boxes where there is sea ice we weight the momentum flux with the ice fraction, so that for grid boxes with 100% sea ice the model is fully coupled. We initialize these simulations at year 1870 from the corresponding ensemble member in CNTRL, and the momentum flux modifications are implemented from year 1871. Thereafter we run the model for 142 years, giving us an ensemble spanning years 1871 to 2012.

The 20CR anomalies are added to the model's daily climatology, in contrast to a fully coupled simulation where the ocean component receives momentum flux from the atmosphere component through the coupler. The anomalies and climatology are both calculated based on the years 1901-2000, where the climatology is calculated from the CNTRL ensemble. Since we are prescribing anomalies the mean state of the model does not change. This method is used to constrain the model variability to observations, while at the same time maintaining an active thermodynamic coupling. In this way, SST is a fully prognostic variable that can freely interact with the atmosphere component of the model. Since both ensembles include the same transient forcing, we can use this experimental setup to separate the impact of dynamical driven Pacific Ocean changes from the radiative forced changes. It should be noted however that the 20CR wind stress anomalies could also include some radiative forced changes, and there could be non-linear interactions between the radiative forced and wind forced responses.

To separate the effect of the tropical Pacific and the extratropical Pacific, we performed two additional 6-member ensemble simulations: XTROP and TROP. XTROP has the same setup as TAU-PAC, but we prescribe momentum flux anomalies only over the region in the Pacific covering 25°N - 60°N with a tapering region of linear weighting of 5° latitude outside the latitudinal boundaries. In TROP, we prescribe momentum flux anomalies only over the tropical Pacific between 20°S - 20°N and from 150°E to the coast of America, with a tapering region of linear weighting of 5° outside the boundaries.

Evaluation of our experimental design

Where there is a strong ocean-atmosphere coupling, for instance in the tropics, our method of partial coupling prescribing wind stress anomalies works well to constrain SSTs. However, since the prescribed wind stress anomalies are not used directly in calculating the surface heat fluxes, the wind-evaporation-SST feedback is not taken into account. At higher latitudes the correlation between observed and simulated SSTs is weaker. The correlation pattern between TAU-PAC and observed SST (Supplementary Fig. 2c and d) matches the masking of the basin, with the Indo-pacific region simulating observed SST variability in TAU-PAC. There is also an area with significant correlation in the tropical Atlantic, similar to the ENSO teleconnection pattern in this region[36].

The main component of extratropical North Pacific SST variability is given by the PDO-index[37]. In TAU-PAC the PDO-index has similar phasing for all realizations, consistent with a wind-driven PDO[37], while there is no consistency between ensemble members of CNTRL (Supplementary Fig. 2a, b). The observed PDO-index increased from 1910 into the early 1940s, but in TAU-PAC the PDO-index lags the observed data by around 5 years in the first half of the simulation. We find a similar delay for the NP-index (Supplementary Fig. 6). The maximum correlation between the observed PDO and the PDO in TAU-PAC for the first half of the simulation is found when the observations lead by 6 years ($r=0.86$, $p=0.005$). The PDO in TAU-PAC follows the observed PDO better in the second half of the simulation with a correlation of 0.93 ($p=0.0002$) at lag zero. The delayed PDO in the first half of the simulation could be due to the response time of the ocean to the prescribed momentum flux that starts in year 1871, or a possible difference in advection timescales in the model compared to reality. The historical PDO-index before 1920 depends on data used[37] and another possible reason for the discrepancies in the beginning of our simulations is that sparse sampling before the 1950s[29] leads to uncertainties in both the PDO index and the reanalysis product used to force the model.

Between 1939-1942 there is evidence of a large El Niño, but this warming in the tropical Pacific is slightly more persistent in TAU-PAC than the observed data used here (Supplementary Fig. 2e and 9). This pronounced equatorial Pacific warming in TAU-PAC can also be seen in the trend pattern in Figure 2c. The difference in the tropical and extratropical warming signals between observations and TAU-PAC (Figure 2a, c) could explain why our model PDO lags the observed PDO. The pronounced El Niño in TAU-PAC might also shift the peak of the PDO-index in the early 1940s a couple of years later compared to the observed PDO-index (Supplementary Fig. 2b). However, due to large uncertainties in the instrumental data[29], it is difficult to pinpoint the exact year of the peak of the early 20th century warming[38]. Nevertheless, the timing of the 1940s dip in the Aleutian Low (Supplementary Fig. 6) and the maximum of the PDO coincides with the El Niño event of the early 1940s and marks the final peak of the early 20th century Arctic warming.

Observational data

We chose the momentum flux from the 20CR in our experiment because it was the longest available product at the time these experiments were initiated. Earlier simulations using this method has shown that the ocean needs years to integrate the implemented wind stress forcing. Furthermore, we have chosen to use the ensemble mean momentum fluxes, anticipating them to be the most accurate. However, the ensemble mean is known to have less variance during the earlier period when observational data are scarce[39]. We avoid some of this issue as the trend in variance is especially pronounced between 40-60°S[39], which is outside the region of partial coupling in TAU-PAC.

For evaluating our model results we have used several other observational data products. For surface temperature, we have used the NASA Goddard Institute for Space Studies Surface Temperature Analysis (GISTEMP)[30], accessed at https://data.giss.nasa.gov/gistemp with 1200km smoothing and using the NOAA Extended Reconstructed SST (ERSST) version 4[40]. For SLP we used the gridded Met Office Hadley Center's mean sea level pressure data set (HadSLP2)[26], and the observed North Pacific index[20] retrieved from https://climatedataguide.ucar.edu/climate-data/north-pacific-np-index-trenberth-and-hurrell-monthly-and-winter. For supplementary figures, we have also used the Hadley Centre Sea Ice and Sea Surface Temperature data set version 1.1 (HadISST)[41], retrieved from https://climatedataguide.ucar.edu/climate-data/sst-data-hadisst-v11, Berkley Earth global surface temperatures[42] provided by http://berkeleyearth.org/data/, and the Nansen-SAT dataset[43].

For our analysis, we have used all grid points for the model data but excluding grid points where there is no coverage in the observed data does not notably change the results from those presented here.

Analysis and statistical methods

The Arctic surface temperature index is given by low-frequency filtered area-averaged surface temperature north of 70°N. The PDO-index is defined as the low-frequency filtered first principle component of detrended SSTs between 20°N-60°N and 120°E-120°W. We use a third-order Butterworth low-pass filter with cut-off frequency of 15 years for low-frequency filtering, and a standard Student t test for assessing significance between ensemble means by considering the spread of each ensemble; for linear correlation coefficients, the effective degrees of freedom based on the auto-covariance is taken into account.

The zonally averaged meridional heat transport is approximated using net longwave and shortwave radiative heat fluxes at the top of the atmosphere and at the surface as well as both latent and sensible heat fluxes at the surface. The atmospheric transport is given by the difference between total heat transport and that estimated for the ocean based on surface fluxes.

The temperature tendency over the Arctic is decomposed using daily model output of atmospheric temperature (T) and three-dimensional wind fields (U, V, Ω) and is given by the following equation

$$\frac{\partial T}{\partial t} = \underbrace{-\frac{1}{a}\left(U\frac{\partial T}{\cos\phi\,\partial\lambda} + V\frac{\partial T}{\partial\phi}\right)} \quad \underbrace{+\,\Omega\frac{T}{\theta}\frac{\partial\theta}{\partial p}} \quad \underbrace{+\,\frac{Q}{c_p}}$$

where a is the Earth's radius, ϕ is latitude and λ is longitude, θ is potential temperature, p is pressure and c_p is the specific heat capacity at pressure p. The warming tendency ($\frac{\partial T}{\partial t}$) of the wintertime temperature response to the Pacific changes are considered for year-to-year and seasonal adjustments. The first term on the right-hand side of the equation is the horizontal advection term, the second term is adiabatic temperature change through vertical motion, and the last term is the diabatic heating given as the residual of the equation by considering the daily temperature tendency. Adiabatic warming (cooling) occurs when there is subsidence (uplift). The terms of the tendency equation are computed first for each grid point at all vertical levels and afterwards averaged over the region of interest.

Data availability

The data that support the findings of this study are available from the corresponding author on request.

References

31 Lindsay, K. *et al.* Preindustrial-Control and Twentieth-Century Carbon Cycle Experiments with the Earth System Model CESM1(BGC). *Journal of Climate* **27**, 8981-9005 (2014).

32 Bleck, R., Rooth, C., Hu, D. M. & Smith, L. T. Salinity-driven thermocline transients in a wind-forced and thermohaline-forced isopycnic coordinate model of the North-Atlantic. *Journal of Physical Oceanography* **22**, 1486-1505 (1992).

33 Iversen, T. *et al.* The Norwegian Earth System Model, NorESM1-M – Part 2: Climate response and scenario projections. *Geosci. Model Dev.* **6**, 389-415 (2013).

34 van Vuuren, D. P. *et al.* The representative concentration pathways: an overview. *Climatic Change* **109**, 5 (2011).

35 Taylor, K. E., Stouffer, R. J. & Meehl, G. A. An Overview of CMIP5 and the Experiment Design. *Bulletin of the American Meteorological Society* **93**, 485-498 (2012).

36 Alexander, M. A. *et al.* The Atmospheric Bridge: The Influence of ENSO Teleconnections on Air–Sea Interaction over the Global Oceans. *Journal of Climate* **15**, 2205-2231 (2002).

37 Newman, M. *et al.* The Pacific Decadal Oscillation, Revisited. *Journal of Climate* **29**, 4399-4427 (2016).

38 Bronnimann, S. Early twentieth-century warming. *Nature Geosci* **2**, 735-736 (2009).

39 He, Y.-C., Drange, H., Gao, Y. & Bentsen, M. Simulated Atlantic Meridional Overturning Circulation in the 20th century with an ocean model forced by reanalysis-based atmospheric data sets. *Ocean Modelling* **100**, 31-48 (2016).

40 Huang, B. *et al.* Extended Reconstructed Sea Surface Temperature Version 4 (ERSST.v4). Part I: Upgrades and Intercomparisons. *Journal of Climate* **28**, 911-930 (2015).

41 Rayner, N. A. *et al.* Global analyses of sea surface temperature, sea ice, and night marine air temperature since the late nineteenth century. *Journal of Geophysical Research-Atmospheres* **108**, (2003). doi:10.1029/2002JD002670

42 Rohde, R. *et al.* Berkeley Earth Temperature Averaging Process. *Geoinformatics & Geostatistics: An Overview* **1:2**, (2013).

43 Kuzmina, S. I., Johannessen, O. M., Bengtsson, L., Aniskina, O. G. & Bobylev, L. P. High northern latitude surface air temperature: comparison of existing data and creation of a new gridded data set 1900–2000. *Tellus A* **60**, (2008).

Acknowledgements

This research was supported by the JPI-Climate / Belmont Forum project InterDec, the Research Council of Norway through the EPOCASA (no. 229774) project, the ERC STERCP project (Grant Agreement No. 648982), and UNINETT Sigma2 with CPU (nn9039k) and storage (ns9039k) resources.

Author Contributions

L.S. and I.B. performed the experiments. L.S. performed the analysis and wrote the manuscript. All authors contributed to discussion, interpretation of the results and editing the manuscript.

Competing Financial Interests statement

The authors declare no competing interests.

Figure Legends

Figure 1 Arctic surface temperature. Low-frequency filtered annual Arctic (70-90°N) surface temperature for GISTEMP[30] (black line) and **a,** the ensemble mean of CNTRL (grey line) and **b,** TAU-PAC (green line). Green (grey) shading indicates the ensemble spread of TAU-PAC (CNTRL). **c**, Change in surface temperature in the Arctic (north of 70°N) between the average over two periods 1911-1920 and 1936-1945 for GISTEMP[30] data (black) and ensemble mean of CNTRL (grey) and TAU-PAC (green) for five month means.

Figure 2 Change in surface temperature and SLP. Change in surface temperature north of the equator in K (**a, b, c**) and SLP north of 20°N in hPa (**d, e, f**) given by the difference between the average over two periods 1936-1945 and 1911-1920 in GISTEMP[30] (**a**) and HadSLP2[26] (**d**), and the ensemble mean of CNTRL (**b, e**) and TAU-PAC (**c, f**) for the cold season (ONDJF). Filled contours indicate significance at a 5% level. Contour levels are shown for every 0.25 K for surface temperature (**a, b, c**) and 0.5 hPa for SLP (**d, e, f**).

Figure 3 Change in vertical temperature and geopotential height in the Arctic. Monthly mean change given by the difference between the average over two periods 1936-1945 and 1911-1920 in temperature (colors) and geopotential height (contours) over the Arctic (north of 70°N) for **a**, CNTRL and **b**, TAU-PAC. Contour levels are shown for every 0.25 K for temperature and for every 20 m for geopotential height. Dashed gray (solid black) lines indicate negative (positive) geopotential height anomalies, and the thick black line indicates the zero line for geopotential height anomalies.

Figure 4 Geopotential height. Change given by the difference between the average over two periods 1936-1945 and 1911-1920 in geopotential height at 53 hPa (**a, b**) and at 510hPa (**c, d**) north of 30°N in CNTRL (**a, c**) and TAU-PAC (**b, d**) for the cold season (ONDJF). Filled contours indicate significance at a 5% level. Contour levels are shown for every 5m and 10m, for 510 hPa and 53 hPa geopotential height, respectively. **e, f** Change (shading) given by the difference between the average over two periods 1936-1945 and 1911-1920 in the Wave 1 component of the eddy geopotential height between 45-75°N in CNTRL (**e**) and TAU-PAC (**f**) for the cold season (ONDJF). Contour lines indicate the climatological wave 1 and are shown at ±60 m and then for every 120m, where gray dashed (black solid) lines are negative (positive). The thick black line indicates the zero line.

Figure 5 Additional experiments. Change in surface temperature in K (**a, e**), SLP in hPa (**b, f**), and geopotential height (GPH) in m at 510 hPa (**c, g**) and at 53 hPa (**d, h**) north of 30°N given by the difference between the average over two periods 1936-1945 and 1911-1920 in the two additional experiments XTROP (**a, b, c, d**) and TROP (**e, f, g, h**) for the cold season (ONDJF). Filled contours indicate significance at a 5% level. Contour levels are shown for every 0.25 K, 0.5 hPa, 5m and 10m, for temperature, SLP, 510 hPa and 53 hPa geopotential height, respectively.

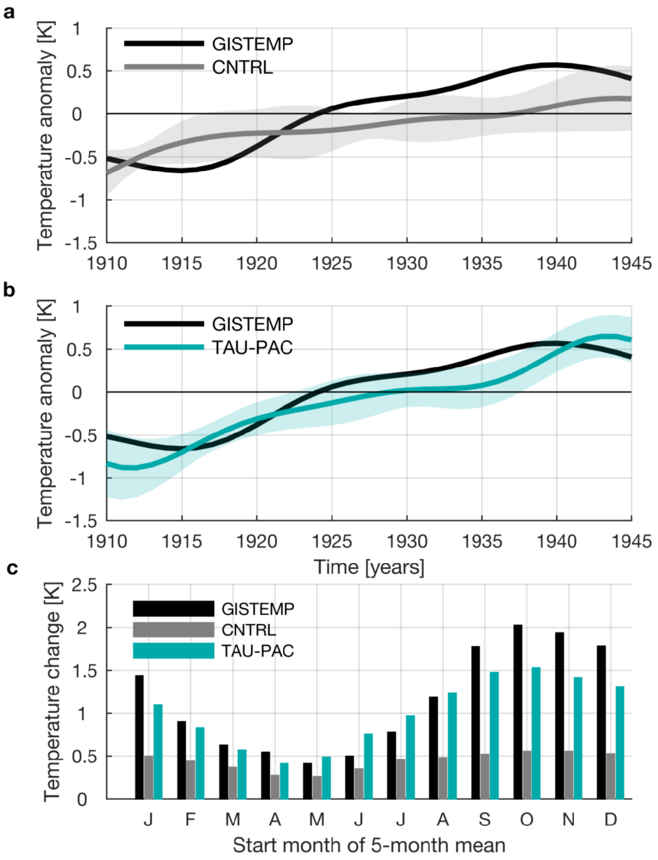
a
Temperature anomaly [K]
GISTEMP
CNTRL
1
0.5
0
-0.5
-1
-1.5
1910
1915
1920
1925
1930
1935
1940
1945
b
Temperature anomaly [K]
GISTEMP
TAU-PAC
Time [years]
c
Temperature change [K]
GISTEMP
CNTRL
TAU-PAC
2.5
2
1.5
1
0.5
0
J
F
M
A
M
J
J
A
S
O
N
D
Start month of 5-month mean

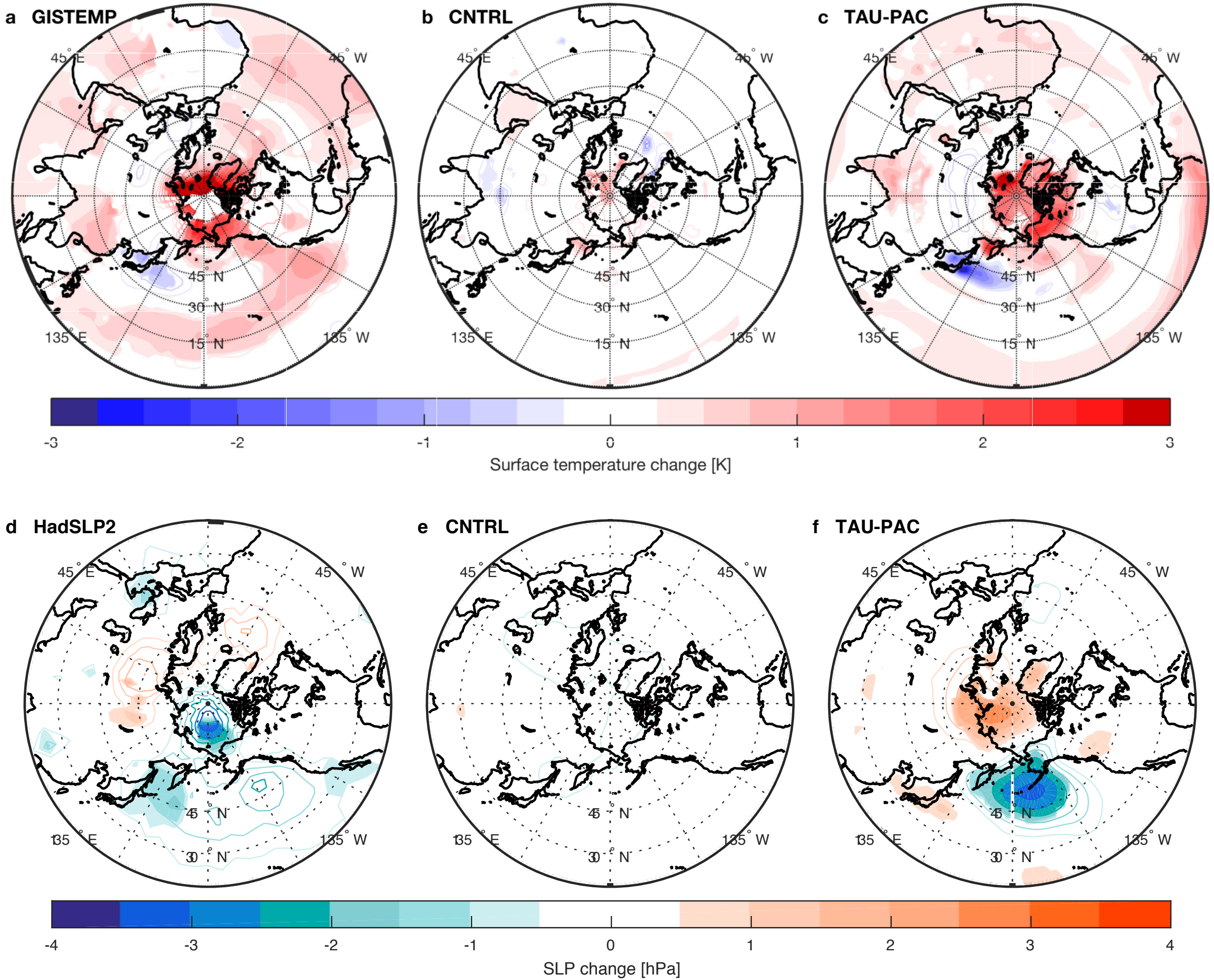
a GISTEMP
b CNTRL
c TAU-PAC
45° E
45° W
135° E
135° W
45° N
30° N
15° N
-3
-2
-1
0
1
2
3
Surface temperature change [K]
d HadSLP2
e CNTRL
f TAU-PAC
-4
-3
-2
-1
0
1
2
3
4
SLP change [hPa]

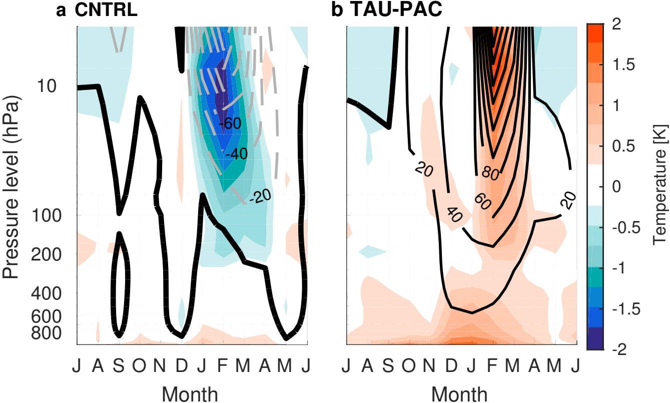

a CNTRL
b TAU-PAC
Pressure level (hPa)
10
100
200
400
600
800
-60
-40
-20
20
40
60
80
20
J A S O N D J F M A M J
Month
Temperature [K]
2
1.5
1
0.5
0
-0.5
-1
-1.5
-2

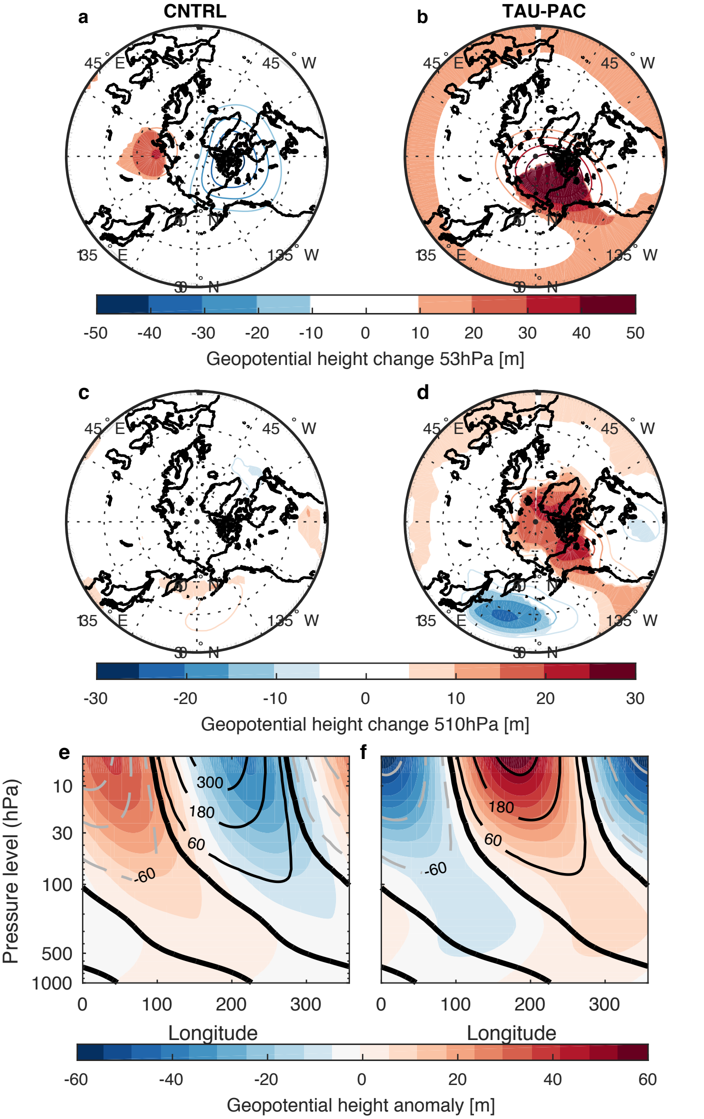

a
CNTRL
b
TAU-PAC
45° E
45° W
135° E
135° W
0° N
90° N
-50
-40
-30
-20
-10
0
10
20
30
40
50
Geopotential height change 53hPa [m]
c
d
-30
-20
-10
0
10
20
30
Geopotential height change 510hPa [m]
e
f
Pressure level (hPa)
10
30
100
500
1000
300
180
60
-60
0
100
200
300
Longitude
-60
-40
-20
0
20
40
60
Geopotential height anomaly [m]

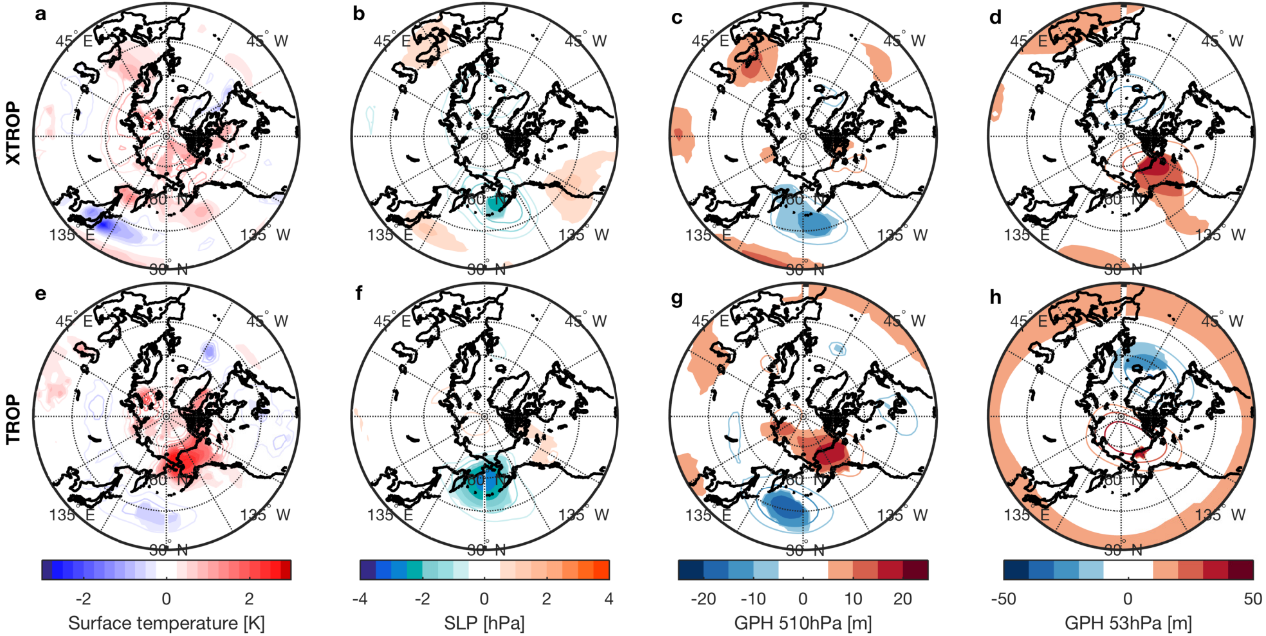

a
b
c
d
e
f
g
h
XTROP
TROP
45° E
45° W
135° E
135° W
30° N
60° N
-2
0
2
Surface temperature [K]
-4
-2
0
2
4
SLP [hPa]
-20
-10
0
10
20
GPH 510hPa [m]
-50
0
50
GPH 53hPa [m]